Thin Solid Films 519 (2011) 1989–1992

Contents lists available at ScienceDirect

Thin Solid Films

journal homepage: www.elsevier.com/locate/tsf

Room temperature ferromagnetism and hopping transport in amorphous CrN thin films

Zhongpo Zhou [a], Shijun Luo [a,1], Yin Wang [a], Zhiwei Ai [a], Chang Liu [a,*], Duofa Wang [b], YoungPak Lee [b]

[a] Key Laboratory of Artificial Micro- and Nano-structures of Ministry of Education, and School of Physics and Technology, Wuhan University, Wuhan 430072, China
[b] q-Psi and Department of Physics, Hanyang University, Seoul 133-791, Republic of Korea

ARTICLE INFO

Article history:
Received 10 January 2010
Received in revised form 9 October 2010
Accepted 29 October 2010
Available online 4 November 2010

Keywords:
Chromium nitride
Ferromagnetism
Electronic transport
Molecular beam epitaxy
Transmission electron microscopy

ABSTRACT

Magnetic and electronic properties of stoichiometric amorphous CrN thin films grown on MgO (001) substrates by radio-frequency nitrogen-plasma-assisted molecular beam epitaxy have been investigated. The magnetic property of the amorphous CrN thin films shows a ferromagnetic behavior even at room temperature, and can be interpreted by the percolation theory of magnetic polaron where we consider Cr^{3+} defects as magnetic impurities which lead to the formation of bound magnetic polarons. The obtained results of electrical conductivity are explained by the variable-range-hopping theory of the Mott and Davis model.

© 2010 Elsevier B.V. All rights reserved.

1. Introduction

CrN has received considerable attention over the past decades due to its high mechanical hardness and corrosion resistance for applications in hard, wear, and corrosion-resistant coatings [1]. In addition, CrN becomes more and more interesting due to its novel magnetic, optical, and electronic properties.

It is known that CrN is paramagnetic (PM) with a NaCl crystal structure at room temperature. At the Néel temperature, reported in a range of 273–283 K, the material undergoes a first order phase transition to antiferromagnetism with an orthorhombic P_{nma} lattice [2,3]. It was considered that the structural distortion was closely related to the magnetic transformation [4,5]. Filippetti et al. [4] reported that CrN was a metal in its PM state but a weak metal in the antiferromagnetic state which agreed well with an earlier experimental work [6]. On the other hand, CrN powder had a band gap of 90 meV as measured by resistivity [7]. It was also reported that the CrN film behaved as a semiconductor (Mott-type insulator) with an optical gap of 0.7 eV [8]. The CrN film grown on MgO (001) by rf-plasma-assisted molecular beam epitaxy (RFMBE) revealed a semiconductor-to-metal phase transition right at the structural phase-transition temperature of 280 K of the bulk [9]. More recently, the CrN/MgO film showed a paramagnetic behavior at low temperatures [10], whereas CrN/sapphire exhibited a ferromagnetic-like response above room temperature. It is therefore still unclear or contradictory how the structural, electrical, and magnetic phase transitions are correlated in this material [11–13]. Especially, the electronic and magnetic properties for the amorphous CrN (a-CrN) have still received little attention to our best knowledge [14–16].

Another motivation for studying the a-CrN films originated from the fact that in Cr-doped, nitride-based dilute magnetic semiconductors (DMSs). CrN is a magnetically relevant compound which might be present as phase segregated clusters and could be responsible for the magnetic properties found in different Cr-doped DMSs, such as Cr-doped GaN [17], AlN [18], and InN [19]. The knowledge of the magnetic property of the a-CrN may be used to confirm or rule out the phase segregation in such DMSs. The structural disorder of the a-CrN films belongs to topological disorder, where the disorder of Cr-doped, nitride-based DMSs is of chemical disorder. The topological disorder and chemical disorder both can break the symmetry of the ordered system at a molecular scale and consequently affect the extended states of the valence and conduction bands, forming localized states [20]. With amorphous materials, according to the location of the Fermi level E_F and the temperature range, the energy range of interest may correspond either to a large density of broken bonds associated with mid-gap states or to disorder-induced localized band-tail states. Understanding of the properties of the a-CrN may be helpful to control the electric and magnetic properties of Cr-doped nitrides.

In this paper, we present experimental evidence on ferromagnetism of the a-CrN thin films grown on MgO (001) substrates by RFMBE whose magnetic moment per Cr atom is closed to that in the bulk CrN at room temperature. The films have atomically smooth surfaces.

* Corresponding author. Fax: +86 27 68752569.
E-mail address: cliu@acc-lab.whu.edu.cn (C. Liu).
[1] Present address: Beijing Institute of Remote Sensing Equipment, Beijing 100039, China.

0040-6090/$ – see front matter © 2010 Elsevier B.V. All rights reserved.
doi:10.1016/j.tsf.2010.10.070

The resistivity measurements exhibit two semiconducting regions, and both can be described by the Mott localization law.

2. Experimental details

The a-CrN thin films were grown on thermally precleaned MgO (001) substrates by RFMBE (SVTA 35V-2) at a substrate temperature of 400 °C with a nitrogen flow rate of 2.65 SCCM. The active nitrogen was produced by a plasma source with an excited radiation frequency of 13.56 MHz and an output power of 345 W. The chromium grains with a purity of 6 N were evaporated by a conventional Knudsen cell and the evaporation temperatures were about 1320 °C measured by a thermocouple. The growth rate was measured out to be roughly 20 nm/h by using the Form Talysurf Profiler (TAYLOR HOBSON, S4C-3D). X-ray photoelectron spectroscopy (XPS, KRATOS XSAM-800) analysis was carried out to qualify the chemical compositions, and identify binding states and the stoichiometry of the a-CrN thin films. A Mg Kα radiation ($h\upsilon = 1253.6$ eV) working at 200 W (12 kV × 16.7 mA) was employed as the X-ray source. The analyzer with a pass-energy of 20 eV for high-resolution spectra was used in a fixed retarding ration mode by applying a retarding ratio of 25. The energy resolution was defined as the full width at half maximum of the Ag $3d_{5/2}$ peak to be about 0.9 eV. All the binding energies of samples have been calibrated by taking the carbon 1*s* peak at 285.0 eV. The morphology of the a-CrN films was measured by using an atomic force microscopy (AFM, SHIMADZU, SPM-9500J3). The microstructures of the films were characterized by using a high-resolution transmission electron microscopy (HRTEM, JEOL JEM 2010 FET) operated at an accelerating voltage of 200 kV. The cross-sectional specimens for the HRTEM observation were prepared by a conventional sandwich technique using mechanical grinding and polishing, and Ar^+ ion milling at a low incident angle of 2–4° with an accelerating voltage of 40 kV in the final stage. The magnetic properties were studied with a commercial superconducting quantum interference device magnetometer (Quantum Design, MPMS XL-7). The magnetization loops were recorded at various temperatures with a magnetic field applied parallel to the sample surface. Before measuring the temperature dependence of the magnetization, the sample was first cooled from 300 to 5 K either under a saturation field of 4 kAm^{-1} (50 Oe) field cooled (FC) or at zero field [zero field cooled (ZFC)]. The volume of the a-CrN samples was calculated from the measured surface areas and thicknesses. The uncertainty of this procedure is about 5% and causes a leading error in determining the magnetization. The electrical resistivity measurements were carried out by the standard four-probe method, using high purity Ag as ohmic contacts on the a-CrN thin films.

3. Results and discussion

Fig. 1(a) and (b) shows the high-resolution narrow-scan core-level XPS spectra of Cr 2*p*, and N 1*s* of the a-CrN specimen. In Fig. 1(a), the two peaks in the spectrum are attributed to the Cr $2p_{3/2}$–$2p_{1/2}$ spin–orbit doublet. Both peaks have a symmetric shape, implying that only one chemical state exists in the film. The Cr $2p_{3/2}$ and $2p_{1/2}$ binding energies are obtained at 575.7 and 586.4 eV, respectively, which are close to those reported Cr^{3+} ions in CrN [21]. The core-level XPS spectrum of N 1*s* shown in Fig. 1(b) also exhibits a symmetric shape. The N 1*s* peak at 396.6 eV is characteristic for N^{3-} species. The stoichiometry can be estimated from the data of core photoemission intensity. The element composition can be quantified by use of X-ray photoelectron intensity values (I_n) and appropriate sensitivity factors (S_n): $\rho_n = I_n/S_n$. S_{Cr} and S_N values of 1.7 and 0.38 were estimated by the procedures similar to ref. [22]. In this way, we got $\rho_{Cr}:\rho_N = 1:1.3$ for the sample after integrating the XPS signals for each element independently.

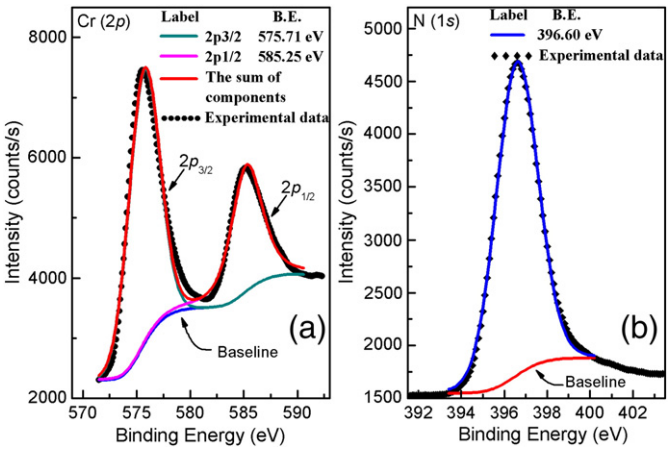

Fig. 1. (a) Cr 2*p* and (b) N 1*s* XPS spectra of the a-CrN.

The cross-sectional HRTEM image in Fig. 2(a) shows a typical microstructure with no long-range order, characterizing an amorphous nature. The fast Fourier transformation (FFT) shown in the inset exhibits the primary halo ring of the amorphous layer. In addition to the amorphous CrN, Fig. 2(a) also appears to show a thin, amorphous layer at the top interface. That layer was about 1 nm thick and could not be an oxide since the XPS survey spectrum did not show any signals of the oxygen. Therefore, the surface oxide can be excluded. Instead, this amorphous layer could be caused by the Ar^+ bombardment during the preparation of the TEM specimen. AFM measurements reveal an atomically smooth surface with a root mean square roughness of about 0.3 nm, as shown in Fig. 2(b).

Fig. 3(a) shows magnetization loops obtained from a 60 nm thick a-CrN film at temperatures of 300 and 10 K in magnetic fields applied parallel to the sample surface up to 800 kAm^{-1} (10 kOe). The signals of the bare MgO substrate have been subtracted so as to show only the contribution of the a-CrN film. The saturation magnetization was found to decrease at 300 K compared with that at 10 K for the a-CrN film. Nitrogen was assumed without magnetic moment (N can have a tiny magnetic moment but it is negligibly small). The moments are expected to be almost all aligned to the magnetic field direction at 10 K and at a magnetic field of 800 kAm^{-1} (10 kOe), confirmed by the fact that the magnetization is almost saturated at that field. Thus the magnetic moment from the magnetization data could be calculated. The measured saturation magnetization (Ms) ~ 14 kAm^{-1} (14 emu/cm^3) corresponds to a moment of 2 μ_B per Cr atom which is smaller than 2.36 μ_B per atom in the antiferromagnetic bulk CrN [2]. It has to be noted that the experimental uncertainty for determining this effective moment depends on the volume of the film, and is expected to be about 5% [10]. The thin film displays a soft nature with a coercive field (Hc) of ~8 kAm^{-1} (100 Oe), and the remnant magnetization (Mr) is lower than 15% of the Ms. Both are comparable to some DMSs, e.g. $In_{0.975}Cr_{0.025}N$ system [19]. Thus the a-CrN thin films grown on MgO are ferromagnetic even at room temperature.

The FC and ZFC curves measured for the a-CrN film are shown in Fig. 3(b) in which the contribution from the MgO substrate has been excluded. A clear separation between the FC and the ZFC curve is visible up to the highest measurement temperature [10], demonstrating the presence of a ferromagnetic ordering. It is worth noting that such a ferromagnetic-like behavior (i.e., magnetic hysteresis and separated FC/ZFC curves) is qualitatively similar to that found in many DMSs, e.g., Cr-doped GaN [17], AlN [18], or InN [19].

The percolation theory of magnetic polaron [23,24] with only one fitting parameter $a_B^3 n_h$, where a_B is the decay length of the magnetic polaron and n_h is the carrier density, can be used to explain the observed magnetic behavior of this disordered system. In this model, the charge carriers are localized and the carriers are electrons. It is

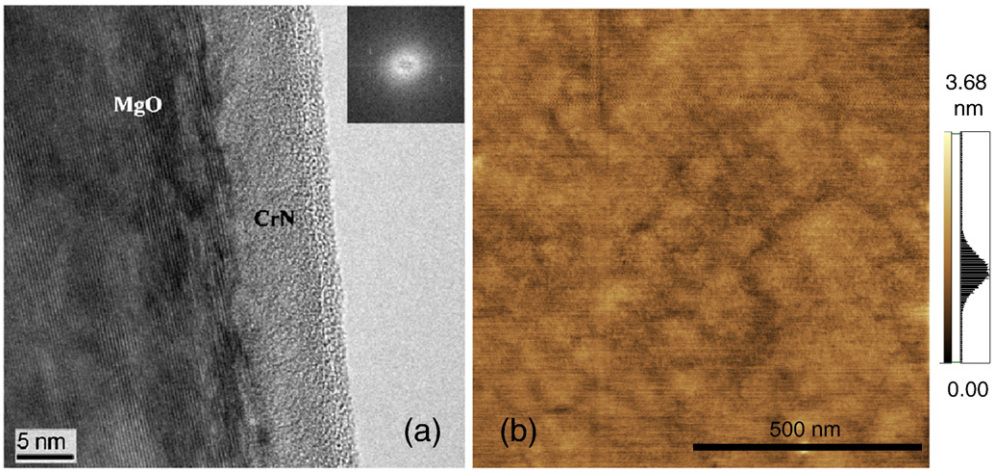

Fig. 2. (a) Cross-sectional HRTEM image of the a-CrN. The inset shows the corresponding FFT derived from a part of the film. (b) AFM morphology of the a-CrN.

remarkable that the FC magnetization curve agrees well with the theoretical prediction as shown in the inset of Fig. 3(b). To understand the physics of the magnetic interaction, two neighboring polarons are considered as shown in Fig. 4, where a bound magnetic polaron consists of one localized carrier, and a number of Cr^{3+} defects as magnetic impurities around the carrier localization center. Although the direct exchange interaction of the localized electrons is antiferromagnetic, the interaction between bound magnetic polarons may be ferromagnetic at large enough concentrations of magnetic impurities [25]. As the temperature is being lowered, the localized carriers of these polarons act on the impurities surrounding them and thus produce an effective magnetic field. The spins of neighboring polarons become aligned to this effective field; and clusters of polarons with the same spin form when the energy minimum is reached. The lower the temperature, the more clusters with even larger sizes are developed. At low enough temperatures, a cluster having the dimensions of the specimen, the so-called "infinite cluster" appears, and the magnetization of the sample acquires some finite value when the spins of the localized carriers are parallel.

The temperature dependence of the electrical resistivity of the a-CrN is shown in Fig. 5. The curve can be classified into three temperature regions. In the first region, the resistivity decreases with increasing temperature up to ~180 K, showing a semiconducting type.

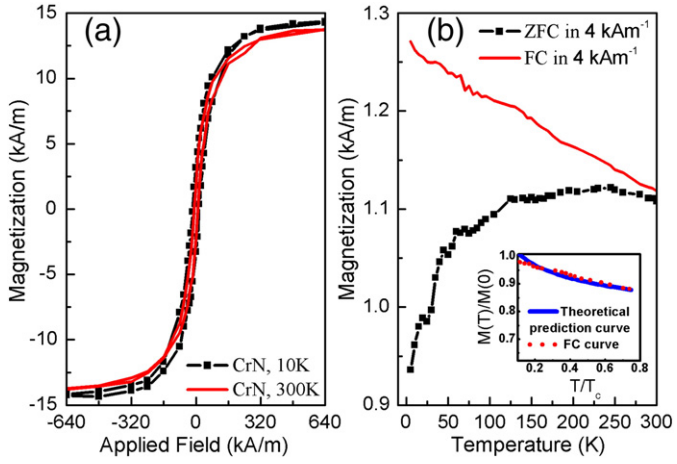

Fig. 3. (a) Magnetization vs applied field at 300 and 10 K of the a-CrN. (b) Magnetization vs temperature at an applied field of 4 kAm^{-1} (50 Oe) of the a-CrN. Both FC and ZFC traces are shown. The inset shows FC (red line) and the theoretical prediction (green line) from magnetic polaron percolation with $a_B^3 n_h = 0.004$.

In the second region, however, it increases up to ~230 K, indicating a metallic type. In the third region, it decreases to ~0.5 Ω·cm up to 300 K, showing again a semiconducting type. This behavior is similar to that of some DMSs like epitaxial $Ga_{1-x}Mn_xAs$ layers ($x = 0.03$) doped by Be with different concentrations [26].

To understand the transport mechanism of the a-CrN thin films, attempts have been made to fit the semiconducting regions either using an activation law $\rho(T) = \rho_0 \exp(E_a/kT)$ or using a localization law $\rho(T) = \rho_0 T^b \exp(T_0/T)^p$, where $p = 1/4$, corresponds to the Mott localization law for variable-range hopping of electrons in a band of localized states. The mean localization energy and the mean hopping range are both proportional to $T_0^{1/4}$, which is the significant parameter. As the exponent (b) in the prefactor is simple and model-dependent and it varies much more slowly than the $\exp(T_0/T)^p$, the T^b factor is generally omitted in the analysis. The hopping process of charge transfer by the phonon-assisted tunneling from occupied to unoccupied electronic states takes place in a localized energy band. By fitting the data, $T_0^{1/4}$ in the first and the third regions is 7.7 and 11.2, respectively. The localization energy is weaker in the lower temperature range meaning that the magnetic disorder plays a large role in the localization, and the low-temperature semiconducting region is not directly caused by the magnetic induction in the sample. Instead, the atomic disorder should account for the semiconducting behavior.

Fig. 5 shows a maximum (hump) around 230 K. This critical behavior of resistivity is commonly observed in magnetic metals and magnetic semiconductors and may be ascribed to the carriers scattering by magnetic spin fluctuation via exchange interaction [27]. The hump height depends on several factors including the concentration of free carriers. Randomly distributed Cr^{3+} defects as magnetic impurities create not only a fluctuating electrostatic potential, but

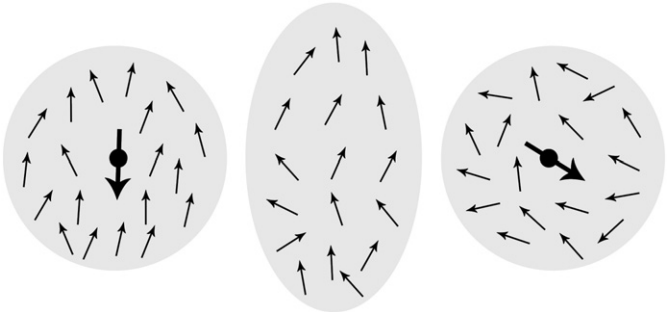

Fig. 4. Interaction of two bound magnetic polarons (after ref. [23]). The polarons are shown with gray circles; small and large arrows show impurity and carrier spins, respectively.

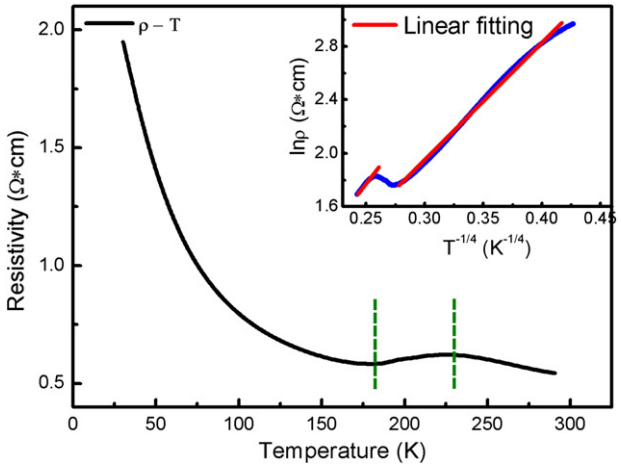

Fig. 5. Temperature dependence of resistivity of the a-CrN thin film. The inset shows the plot of lnρ vs $1/T^{1/4}$.

also static fluctuations of the magnetization, which additionally contribute to the scattering of the charge carriers.

4. Conclusions

In summary, we have deposited the a-CrN thin films with atomically smooth surfaces on MgO (001) substrates by RFMBE which exhibit strong ferromagnetism up to room temperature, comparable to that of the bulk antiferromagnetic CrN. The percolation theory of magnetic polaron taking into account both disorder and strong magnetic interaction originated from the localized carriers can be used to explain the observed magnetic behavior. The resistivity measurement shows two semiconducting regions, and both can be described by the Mott localization law. The magnetic disorder plays an important role in the localization in the high-temperature range. However, in the low-temperature semiconducting region, the atomic disorder dominates. The hump of the resistivity around 230 K may be ascribed to the scattering of carriers by magnetic spin fluctuation via exchange interaction.

Acknowledgments

The authors are grateful to Y. Zhang of Prof. J. Shi' group for the resistivity measurements and thank Dr. Q.M. Fu, Dr. T. Peng, and Y. Pan for their help in the specimen preparation. This work is supported by the National 973 Program No. 2007CB935304 and by the NSFC Nos. 10775110, 11074192 and J0830310.

References

[1] B. Navinšek, P. Panjan, I. Milošev, Surf. Coat. Technol. 97 (1997) 182.
[2] L.M. Corliss, N. Elliott, J.M. Hastings, Phys. Rev. 117 (1960) 929.
[3] A. Mrozińska, J. Przystawa, J. Sòlyom, Phys. Rev. B 19 (1979) 331.
[4] A. Filippetti, W.E. Pickett, B.M. Klein, Phys. Rev. B 59 (1999) 7043.
[5] A. Filippetti, N.A. Hill, Phys. Rev. Lett. 85 (2000) 5166.
[6] J.D. Browne, P.R. Liddell, R. Street, T. Millis, Phys. Status Solidi A 1 (1970) 715.
[7] P.S. Herle, M.S. Hedge, N.Y. Vasathacharya, S. Philip, M.V.R. Rao, T. Sripathi, J. Solid State Chem. 134 (1997) 120.
[8] D. Gall, C.-S. Shin, R.T. Haasch, I. Petrov, J.E. Greene, J. Appl. Phys. 91 (2002) 5882.
[9] C. Constantin, M.B. Haider, D. Ingram, A.R. Smith, Appl. Phys. Lett. 85 (2004) 6371.
[10] A. Ney, R. Rajaram, S.S.P. Parkin, T. Kammermeier, S. Dhar, Appl. Phys. Lett. 89 (2006) 112504.
[11] K. Inumaru, K. Koyama, N. Imo-oka, S. Yamanaka, Phys. Rev. B 75 (2007) 054416.
[12] C.X. Quintela, F. Rivadulla, J. Rivas, J. Appl. Phys. Lett. 94 (2009) 152103.
[13] A. Herwadkar, W.R.L. Lambrecht, Phys. Rev. B 79 (2009) 035125.
[14] W.R.L. Lambrecht, M.S. Miao, P. Lukashev, J. Appl. Phys. Lett. 97 (2005) 10D306.
[15] M.S. Miao, W.R.L. Lambrecht, Phys. Rev. B 72 (2005) 064409.
[16] P.A. Bhobe, A. Chainani, M. Taguchi, T. Takeuchi, R. Eguchi, M. Matsunami, K. Ishizaka, Y. Takata, M. Oura, Y. Senba, H. Ohashi, Y. Nishino, M. Yabashi, K. Tamasaku, T. Ishikawa, K. Takenaka, H. Takagi, S. Shin, Phys. Rev. Lett. 104 (2010) 236404.
[17] M. Hashimoto, Y.-K. Zhou, M. Kanamura, H. Asahi, Solid State Commun. 122 (2002) 37.
[18] R.M. Frazier, G.T. Thaler, J.Y. Leifer, J.K. Hite, B.P. Gila, C.R. Abernathy, S.J. Pearton, Appl. Phys. Lett. 86 (2005) 052101.
[19] P.A. Anderson, R.J. Kinsey, S.M. Durbin, A. Markwitz, V.J. Kennedy, A. Asadov, W. Gao, R.J. Reeves, J. Appl. Phys. 98 (2005) 043903.
[20] P.W. Anderson, Phys. Rev. 109 (1958) 1492.
[21] P. Marcus, M.E. Bussell, Appl. Surf. Sci. 59 (1992) 7.
[22] C.D. Wagner, W.M. Riggs, L.E. Davis, J.F. Moulder, G.E. Muilenberg, in: G.E. Muilenberg (Ed.), Handbook of X-ray Photoelectron spectroscopy, Perkin-Elmer Corp., Physical Electronics Division, Eden Prairie, Minnesota, USA, 1979, p. 188.
[23] A. Kaminski, S.D. Sarma, Phys. Rev. Lett. 88 (2002) 247202.
[24] J.M.D. Coey, M. Venkatesan, C.B. Fitzgerald, Nat. Mater. 4 (2005) 173.
[25] P.A. Wolff, R.N. Bhatt, A.C. Durst, J. Appl. Phys. 79 (1996) 5196.
[26] S.U. Yuldashev, H. Im, V.S. Yalishev, C.S. Park, T.W. Kang, S. Lee, Y. Sasaki, X. Liu, J.K. Furdyna, Appl. Phys. Lett. 82 (2003) 1206.
[27] S. von Molnár, T. Kasuya, Phys. Rev. Lett. 21 (1968) 1757.